Journal of Building Engineering 67 (2023) 106008

Contents lists available at ScienceDirect

Journal of Building Engineering

journal homepage: www.elsevier.com/locate/jobe

ITZ microanalysis of cement-based building materials with incorporation of siderurgical aggregates

A. Aghajanian [a], A. Cimentada [a], M. Fayyaz [b], A.S. Brand [c], C. Thomas [a, *]

[a] LADICIM (Laboratory of Materials Science and Engineering), University of Cantabria. E.T.S. de Ingenieros de Caminos, Canales y Puertos, Av./Los Castros 44, 39005, Santander, Spain

[b] GEURBAN Research Group, School of Civil Engineering, University of Cantabria, 39005, Santander, Spain

[c] Charles E. Via, Jr. Department of Civil and Environmental Engineering, Virginia Polytechnic Institute and State University, 305A Patton Hall, Blacksburg, VA, 24061, USA

ARTICLE INFO

Keywords:
Microstructure
SEM
TEM
SPM
ITZ
Siderurgical aggregates

ABSTRACT

With the depletion of natural resources, it is essential to use recycled materials and industrial wastes to adapt the expanding building sector to the environment. Slag from electric arc furnaces is one example that can be used as a siderurgical aggregate in concrete production. Studying the interfacial transition zone between the aggregate and the binder is necessary because the reaction between the aggregate and the binder can significantly impact the concrete's microstructure and mechanical properties. In order to examine any concrete sample with any physical or chemical structure, this study introduces the instruments used to conduct these studies and the methods for preparing concrete samples for the desired area. The results show that solvent exchange with Ethanol is the best method for draining water from the inner surface of the sample in the interfacial transition zone (ITZ) with minimal destruction. Also, the kind of sample and its information determine the type of coating that should be applied. Gold is the best choice to examine the topography of the sample surface because it has a higher electron return coefficient than other elements and produces images of higher quality. The epoxy with a viscosity of 550 cP (20 °C) or 150 cP (50 °C), a maximum curing temperature of 50 °C, a curing time of 8 h, and an epoxy-to-hardener ratio of 25 to 3 g is the best configuration for having the best sample for microanalysis.

1. Introduction

During 1956 research into concrete, Jacques Farran found a region with distinct characteristics in the space between the cement paste and the aggregate. Additionally, he found that a concrete transition zone has several detrimental effects, such as a lack of adhesives [1–4] and an increase in some non-adhesives in ITZ [5,6]. For instance, ettringite and calcium hydroxide crystals, which lack adhesive properties, are more prevalent in ITZ than in other concrete areas [7,8]. In contrast, calcium silicate hydrate gel, a cementitious material with adhesion properties, is less present than in the bulk paste [9]. Furthermore, compared to the bulk microstructure, the ITZ between cement paste and aggregate also has an increased porosity [10,11], decreased compressive and tensile strengths [12–14], and increased permeability [15,16], all of which result in concrete being more susceptible to sulfate and chloride penetration and eventual deterioration [17–19]. Researchers have been working to reduce the detrimental characteristics of the cement paste and aggregate transition region for roughly 60 years and have employed various techniques [20,21] (see Table 1).

* Corresponding author.
E-mail addresses: ali.aghajanian@unican.es (A. Aghajanian), anaisabel.cimentada@unican.es (A. Cimentada), maryam.fayyaz@alumnos.unican.es (M. Fayyaz), asbrand@vt.edu (A.S. Brand), carlos.thomas@unican.es (C. Thomas).

https://doi.org/10.1016/j.jobe.2023.106008
Received 11 November 2022; Received in revised form 9 January 2023; Accepted 30 January 2023
Available online 2 February 2023

Table 1
Six-step information for sample polishing.

Polish surface steps	Step 1	Step 2	Step 3	Step 4	Step 5	Step 6
Abrasive (μm)	186	46	30	18	10	6
Water	on	on	on	on	on	on
Speed (rpm)	150	150	160	170	180	190
Pressure (kg/cm^2)	8.77	8.46	8.15	8.15	7.75	7.44
Time (min)	2:00	2:00	2:30	4:00	4:00	5:00

ITZ is the region around each aggregate particle where the microstructure is changed by aggregate presence. The "wall effect," brought on by the compacting of anhydrous cement grains against the comparatively flat aggregate surface, is thought to be the origin of ITZ [1,3,22]. The ITZ is frequently thought to be 30 μm thick from the edge of the aggregate [23]. For the ITZ area's structure, some models have been put forth to date, the most well-known of which views the region as a uniform shell [24–27]. However, the materials' properties and porosity are more similar to the matrix mass in the transfer area's boundary regions [28]. This boundary area lies between ITZ, and the matrix mass of five μm and has a thickness of approximately [24,25,29–31].

Steel slag can be converted into siderurgical aggregates (SA) through a process and used for internal metallurgical [16], road building [17], cement, and concrete (eco-concrete) [16,18–20]. Slags from steel-making processes, such as electric arc furnaces [32–34], are of particular interest for their potential to yield equivalent or better concrete performance relative to natural aggregates [34–37]. However, the properties of steel furnace slags will vary, thus resulting in concretes with variable mechanical and durability performance [38–40].

While the ITZ has been studied for decades with natural aggregates, less attention has been given to recycled, waste, and by-product aggregates. As parts of the world experience a depletion of quality aggregate stockpiles [41–44], recycled aggregates need to become a stronger focus for research. Furthermore, the ITZ of concretes with steel furnace slag will be variable [45], necessitating studying the ITZ of concretes with these materials. Furthermore, ITZ is one of the weakest concrete areas; a halo surrounding the aggregate is very prone to cracking [1,18]. Therefore, the ITZ area is critical to understanding the mechanical behavior of concrete. Finally, there is no specific standard for making and preparing samples needed for microscopic photography. In some cases, only a minimal sample is available, and errors in making and processing the sample before photographs can lead to the loss of the sample. Therefore, the present research has been done to minimize manufacturing error and waste of time to obtain the desired result and familiarize with the process of doing these things. This study can be considered this way because in most studies conducted, the method used and its effects for making and preparing samples by a conductive or epoxy coating method have yet to be thoroughly investigated. Moreover, according to the results obtained in this study, this directly affects the results of the ITZ analysis.

2. Background

A light microscope, or optical microscope (OM), is the most conventional type. Light microscopes are often non-invasive, inexpensive, and durable, leaving the item being imaged unaltered. Light microscopy comes in a wide variety. However, they usually cannot identify details and objects smaller than about 0.1 mm (100 μm) [46,47]. A microscope's resolution is its capacity to distinguish two features that are spaced a certain amount apart as distinct image objects. The wavelength of visible light radiation, which varies from 400 nm to 700 nm, determines the resolution limit for a light microscope as an intrinsic characteristic [46,48]. In an OM, it may be possible to increase the magnification of images by changing the curvature of the surface of the lenses (degree of concavity and convexity) and their number. However, due to the long wavelength of light, images practically lose their sharpness at magnifications above 2000. For example, seeing organic cells' structures requires 10,000× magnification, which is impossible with a light microscope with visible wavelengths [49]. The most popular types of microscopes used to examine cement-based materials are the metallographic microscope (reflected light) and the petrographic microscope (transmitted light) [50], and a smooth polished surface is necessary for viewing in both circumstances [51].

In contrast to OM, electron microscopy uses electrons to image, which have a wavelength that is orders of magnitude smaller than visible light, allowing the magnification of electron microscopy to be on the order of 1,000,000x or more. Depending on the kind of microscope being used, there are two general classifications of electron microscopy: scanning electron microscopy (SEM) and transmission electron microscopy (TEM). All SEM and TEM microscopes produce an extremely focused electron beam that strikes the specimen inside a vacuum chamber. On the other hand, TEM microscopes are primarily designed to investigate the interior structure of specimens. In contrast, SEM microscopes are primarily geared to analyze material surfaces, not unlike reflected light microscopes [47,52].

By SEM method, two-dimensional images of the sample structure are obtained. When electrons collide with a sample surface, the material's electrons are excited, and when they return to their original orbit, they are emitted as electrons from the sample's surface and collected and analyzed by a detector [53,54]. These emitted electrons are known as secondary electrons. The interaction of the primary electron beam with the sample surface will also produce other electrons, including backscattered electrons and Auger electrons, as well as characteristic X-rays. The detection of specific electrons and X-rays from the sample are used to characterize various properties of the material, such as chemical composition, surface topography, morphology, crystallography, and electrical and magnetic properties. Concrete has pores, which is why liquids and gases can easily penetrate it. As a result, the concrete surface exposed to air is carbonated almost immediately, and a micron-thick carbonate layer is formed on it. Therefore, the vacuum technology must

cover the sample's surface. Also, in the polishing stage, the sample's surface should be polished well to remove the carbonized layer, if there is any.

Ignition of gases and the possibility of ionizing electrons in the gas environment, the possible discharge of the charge, leading to instability of the beams [55]. The brightness and sharpness of each point in the SEM image depend on the intensity (number) of electrons returning from the sample surface, which is also strongly dependent on the local quality of the surface [56]. This way, a measure of the elevation and height of the surface can be obtained. In the obtained images, the light points indicate the raised surface, and the darker points indicate the surface holes and depressions. Fig. 1 shows the internal and external views of an SEM device.

A significant section of the material is exposed to an electron beam at the TEM [47]. The image is produced when an electron-sensitive screen is exposed to the passing electron beam. The sample's thickness must be less than 100 nm for the electron beam to pass through [9,57]. In some studies, samples with a thickness of up to 200 nm have been used with this method [58]. However, it should be noted that the quality of the obtained results decreases with the increase in thickness [59–61]. Because of this, it is necessary to thin the sample to take pictures of non-powder samples, which can be extremely challenging in some circumstances. Therefore, powder samples with particle size less than 100 nm do not require special preparation [62].

Scanning Probe Microscope (SPM) is a general term for a set of techniques that scan the surface of a material with resolution on the nanometer scale or even less than angstroms and produce topographical images or maps of a physical or chemical property of the surface of the material [63]. Prepares In this technique, like other scanning microscopy methods such as SEM, the surface of the sample is scanned by a needle or probe, and by measuring and processing the signal obtained from different points of the scanned surface on the sample, the image of that surface is prepared [64,65]. The resolution and magnification of the scanning probe microscope are better than conventional electron microscopes, and it also provides the ability to produce 3D images of atoms [66]. In addition to creating an image, this technique also allows the movement of atoms. Unlike most common electron microscopes that require vacuum and sample preparation, scanning probe microscopes work in addition to vacuum, in air, or under the surface of a liquid, with minimal sample preparation (and in some cases without the need for preparation) [63,65].

Along with the possibility of measuring and using different signals for imaging, it examines a wide range of hard, soft, conductive, semiconductor, insulating, magnetic, and materials [64,66]. The resolution of microscopic images is determined according to the type of beam used. For example, a resolution of about one μm or even 200 nm can be achieved using optical microscopes, and a resolution of about 1 nm to a few Angstroms can be achieved using electron and STM microscopes. In this regard, the vertical and horizontal accuracy of some of the essential microscopic methods is shown in Fig. 2. As seen in Fig. 2, many methods overlap, especially in the range of 10–100 nm. However, these methods do not necessarily produce images from the same part of the sample. For example, SEM and TEM both have much overlap, but the former images are of the surface, and the last images are of the interior of the material. In this regard, the depth of focus and accuracy of microscopic methods are shown in Fig. 2. Also, in Fig. 3, the difference in the hardware of the three mentioned methods of SEM, TEM, and SPM is stated. As it is known, the two SEM and TEM methods are very similar in terms of how the hardware works.

According to Fig. 4, image (a) is related to the backscattered electron imaging mode (b) is related to SEM imaging in the secondary electron mode and image [54,55,70]. In the case of the secondary electron, the position and height of the sample surface are well-defined, and crystals with particles between them can be seen. Return electron images, the post and surface altitudes are not well known, but a clear contrast is observed between the particles between the crystals, indicating that the material of the particles between the crystals is different from that of the crystals. Brighter areas in imaging mode are related to materials and compounds with higher atomic numbers [56,71].

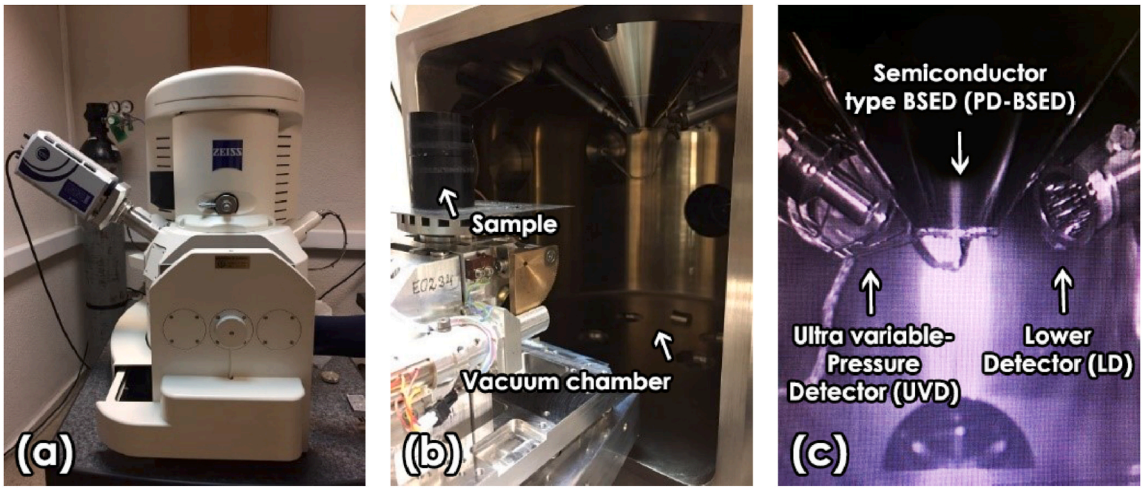

Fig. 1. Internal and external view of SEM device: Exterior of the instrument (a), vacuum area sample position (b), and semiconductor and detector components (c).

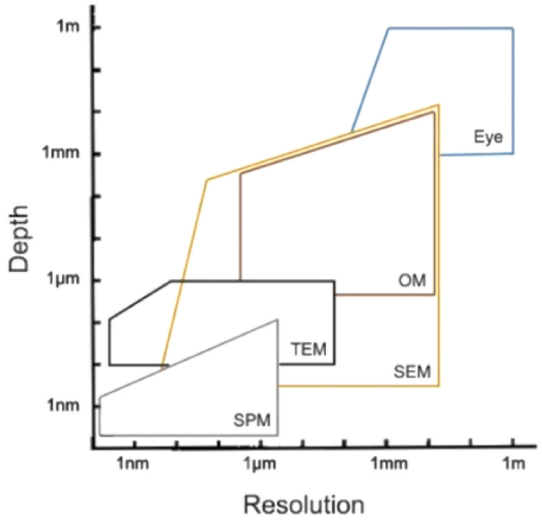

Fig. 2. The depth of focus and accuracy of microscopic methods [67].

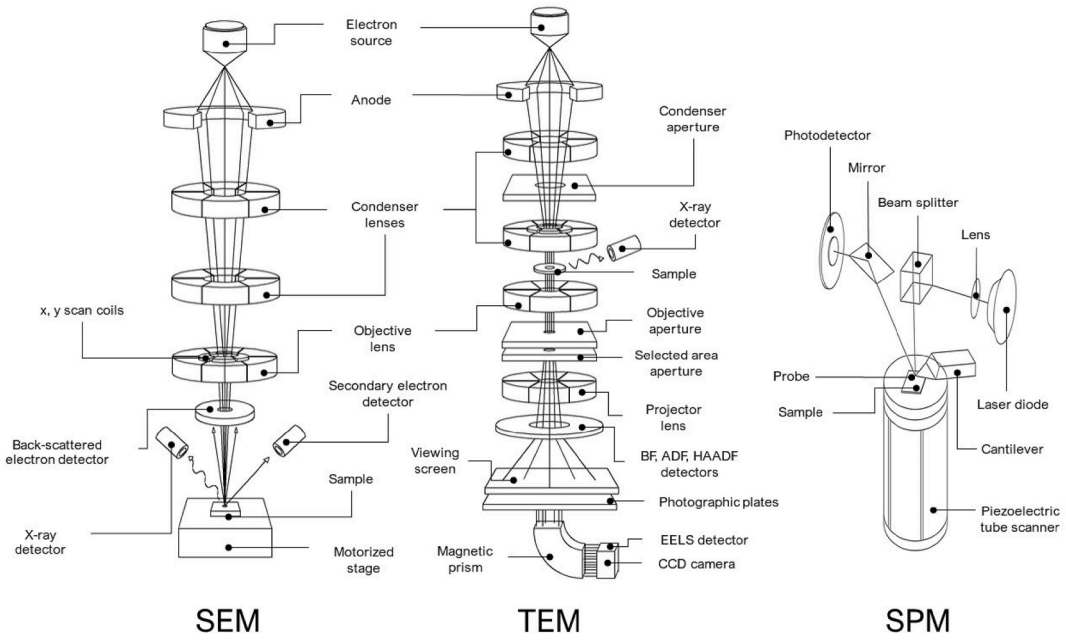

Fig. 3. The difference in the hardware of the three Imaging by electron microscopy methods of SEM, TEM, and SPM [68,69].

3. Sample preparation

There are two methods to prepare and cover the surface of the samples. One method is to cover the surface of the sample with gold or gold coating (GC), and another is to use epoxy resin to cover the sample's surface or epoxy coating (EC) [72,73]. In the GC method, the distance between the sample and the target, typically used to modify the layer's thickness from a flow chart in terms of time, can be controlled by three factors in this method: flow, time, and the thickness of the applied coating. For low magnifications (between 5 and 10,000 times), pure gold is typically used, followed by gold/platinum for medium magnifications (between 10,000 and 50,000 times) and platinum for magnifications greater than 50,000 times [74]. In the EC method, which is a family of two-component resins and includes "resin base" and "hardener" in a particular proportion, according to its formulation and application, these two components must be mixed [75,76]. The resin base (A) is the main component that requires the hardener of component (B) [73,77]. There are different resin bases, most of which are available and suitable samples of the "Bisphenol-A″ type [78–80]. The most widely used epoxy hardeners are divided into two main groups: polyamine hardeners and polyamide hardeners [80–83]. The hardeners used to make EC samples are polyamine type, which are usually diluted and colorless [79,84,85]. The resin used in this research is the Epofix type. This epoxy has a viscosity of 550 cP (20 °C)/150 cP (50 °C), a maximum curing temperature of 50 °C, a curing time of 8 h, and an epoxy-to-hardener ratio of 25 to 3 g.

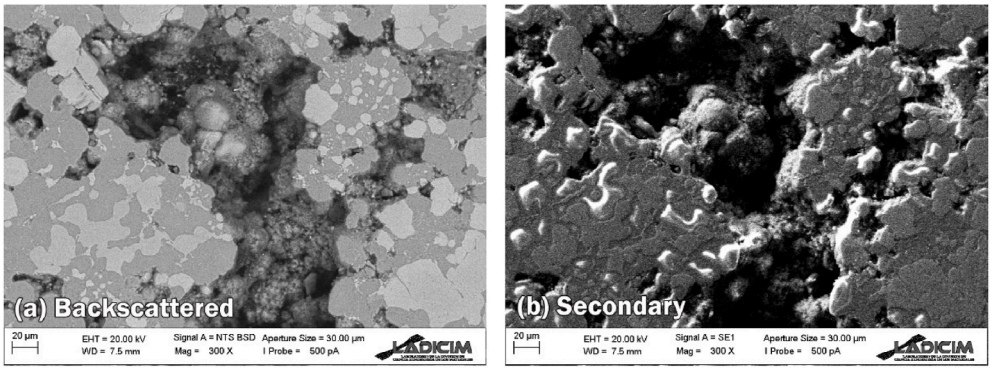

Fig. 4. SEM image in the secondary and backscattered electron modes.

3.1. Sample drying process

Structured water, gel water, and capillary water are some types found in hydrated cement. Crystallization water and chemically bound, non-evaporable water that can only be extracted through hydrate decomposition are examples of structural water Decomposition [86,87]. Gel water is kept on the surface of the top cement hydration product, C-S-H gel, by capillary tension and strong hydrogen bonding [88]. Evaporation at ambient or reduced pressure, at ambient or elevated temperature, removes this water from nanometer-scale pores. As a result, the unbound water inside the pores is available for reaction during hydration, known as capillary water [89–91]. Therefore, capillary water must be eliminated when stopping hydration and drying cement paste. The composition and microstructure of many cement hydrates may change if the first two types of water are removed, which could be undesirable. Because they have the highest relative surface area, the smallest gel pores make it difficult to replace or remove water [92,93]. In addition, the temporary capillary pressure caused by the stresses associated with the surface tension of the receding water menisci may cause the sample to shrink and change the fine pore structure of the cement paste [87,89].

Drying-related phenomena include desaturation, the reaction of hydration products with solvents, desorption, and dehydration. However, these methods can cause microcracking, changes in capillary porosity, the collapse of gel pores, and mineralogical transformations [86,91–93]. Direct drying (removing water by evaporation or sublimation) and solvent exchange are the two main techniques for stopping hydration and removing water [91,92]. Water is eliminated using all direct drying methods by turning it into vapor. The water inside the cement paste will be liquid if the specimen is at room temperature and atmospheric pressure before the drying technique is used. The interfacial tension produces capillary suction at the boundary between the liquid and gas phases. It can lead to microcracking and the collapse of the delicate microstructure of the cement paste [92]. The ideal solvent would have a small molecular size to replace the water in the smallest pores when using the solvent exchange method. In addition, a lower boiling point (higher vapor pressure) makes it easier to remove the solvent without having to heat the mixture to levels that might change the cement's structure or composition. Finally, the solvent must be soluble to replace the water in the pores and stop hydration; effective hydration arrest can be achieved by diffusing the water quickly. In addition, reduced surface tension can reduce drying-related pore structure damage.

This study used the solvent exchange method to dry the samples. The solvent used is Ethanol, which is abbreviated as EtOH. Its chemical formula is CH_3CH_2OH, its molecular weight is 46.07, its specific gravity is 0.789, Insoluble in water and its boiling point is 78.4 °C. The specimen is weighed before submerging it in an organic liquid to replace the solvent. The solvent diffuses into the paste during immersion, taking the place of the pore solution. The change in the specimen's mass is a gauge for the solvent's penetration. After the weight settles, the solvent evaporates at room temperature, higher temperatures, under atmospheric pressure, or in a vacuum.

3.2. Preparation of samples for gold coating (GC)

On the surface of non-conductive samples like concrete, standard coatings are frequently made of gold, gold/palladium, platinum, or carbon [74]. The kind of sample and the kind of information needed from the sample determine the type of applied coating that should be used. When making this decision, it is essential to consider the applied coating material's electrical conductivity, secondary electron emission speed, chemical stability, and cost [94]. In addition, it should be noted that coatings of chromium, copper, aluminum, and different kinds of refractory metals, such as tungsten and tantalum, can also be used as conductive coatings on the surface of the samples in exceptional circumstances and according to the results required from the sample [72,95]. Gold or gold/palladium coating is typically used to examine the topography of the sample surface because it has a higher electron return coefficient than other elements and produces images of higher quality.

One of the most critical points to pay attention to when applying a suitable coating on the surface of semi-conductive and non-conductive samples is the thickness of the applied coating, which has a direct relationship with the coating method. The thickness of the applied coating layer should be only enough to create a suitable conductive path for the flow of electrons. On the other hand, the applied coating should be thin enough not to darken and disappear details related to the topography of the sample surface. On the other hand, the gold particles are entirely fine-grained and adhere to the sample's surface more uniformly. Because the gold element overlaps the most with elements like phosphorus and sulfur in the results of the chemical analysis of the sample and decreases the accuracy of the percentage of the elements in the sample [96,97], carbon coating is chosen over gold coating for samples that need to

provide results for the chemical composition [98–100]. Carbon has a lower atomic number than gold and therefore provides more accurate results for the chemical analysis of the sample [8,101]. Fig. 5 shows the sample coating and purity.

3.3. Preparation of samples for epoxy resin coating (EC)

The samples must be prepared with the cutting device to the appropriate size required to analyze the ITZ of the samples. One standard size is cylindrical, with 6 mm in height and 20 mm in diameter. After cutting with a high-precision saw, the sample is dried to prevent the progress of hydration reactions, often by solvent exchange procedures [102,103]. After drying, the sample is implanted in low-viscosity epoxy resin [94,99]. The constituent components of the resin material consist of two parts. One is the resin material itself, and the other is the resin hardener, which is added to the first material according to the manufacturer's instructions and then poured into a mold containing the sample. Because there are resins in the market with different degrees of transparency, colorless and high-transparency resins should be used. The transparency of the resin depends on the quality of the raw materials of this material, so if low-quality materials are used, the resin changes color after hardening and changes color from colorless (glass) and becomes cloudy the color. It turns yellow. According to the given explanations, care must be taken to use a high-purity resin [14,74]. Otherwise, it is impossible to check ITZ by changing the color, and the sample will not be used due to the impossibility of changing the resin used. It should be noted that before adding the resin to the mold, the two components must be thoroughly mixed in another container and then added to the mold.

Epoxy impregnation stabilizes the sample by sealing pores and voids, allowing it to withstand pressures exerted during grinding and polishing while conserving the original microstructure and component distribution by minimizing particle debonding from softer phases [104]. Fig. 6 shows the four steps of sample preparation. It should be noted that if the low-quality resin is used at this stage, it changes color and becomes cloudy.

Air bubbles are produced when resin and hardener are mixed, and the number of bubbles produced depends on the resin used and the hardener used. The number of air bubbles does not affect future tests, but care must be taken not to produce large bubbles as they may prevent the resin from reaching all parts of the concrete. The application of a vacuum can aid with the removal of bubbles [105]. There is no standard for removing air bubbles, so here is an experimental method that has been used in several previous pieces of research and has been successful [105]. It is crucial to stir the mixture slowly, as rapid stirring causes many bubbles in the resin. The mixture should rest for 2–3 min so that the bubbles have time to clear [105]. After preparing the resin and transferring it to a particular container in the vacuum tank (a), the tank door is closed, and the tank's air release valve is opened (b) so that all the air inside the tank is removed and the tank is vacuumed. The tank remains under a pressure of 20 in. Hg (0.67 bar) in vacuum (c) until a bubble is observed and the vacuum operation is stopped. After adding the resin, the sample is placed at room temperature (20 °C - 25 °C) for 48 h. Fig. 7 shows the vacuum stages of the samples.

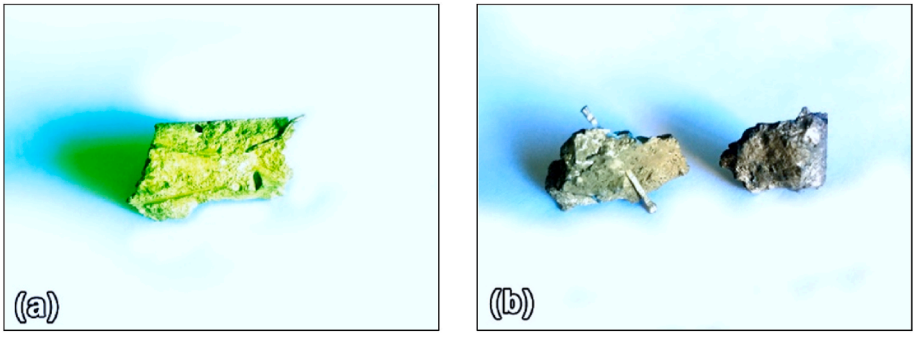

Fig. 5. Acceptable (a) and unacceptable (b) samples show the amount of coating and purity of the gold used. (For interpretation of the references to color in this figure legend, the reader is referred to the Web version of this article.)

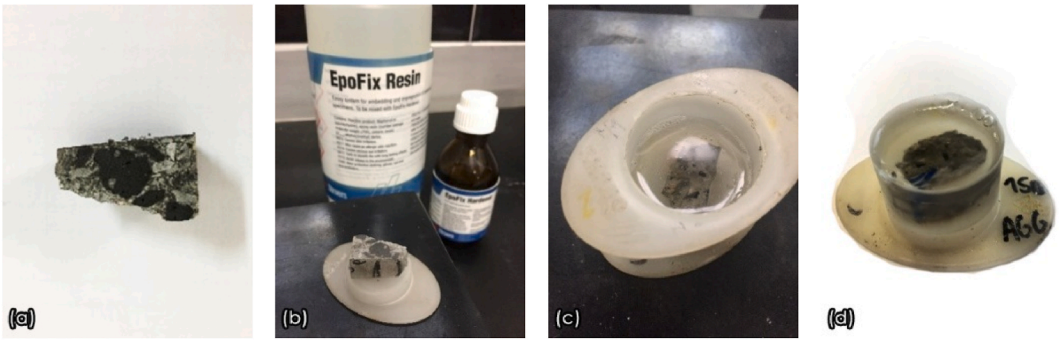

Fig. 6. Sample cutting (a), resin material components (b), sample processing (c), fabricated sample (d).

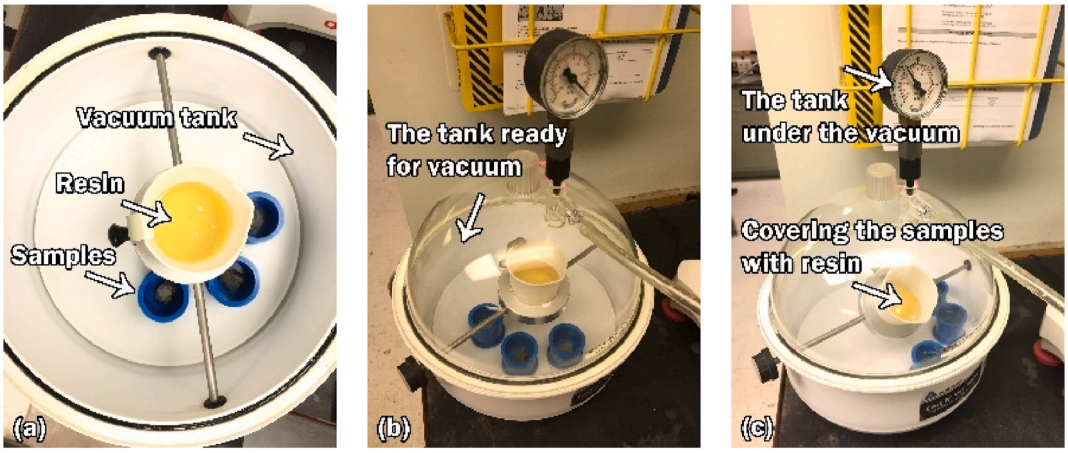

Fig. 7. The vacuum stages of the samples.

3.4. Cutting and polishing samples

After the above step, the sample is cut to reach a thickness of 6–25 mm. The thickness of the sample depends on the thickness required by the device to polish the samples [105]. During the above steps, the sample's surface must be polished to have a high-resolution image without scratch lines created by cutting on the surface of the resin. If this step is not done, black hatching lines will appear on the surface of the sample, resulting from scratches caused by the blade surface of the cutting device [102,105].

In order to have a polished surface without scratches (noise) by the polishing device, four parameters must be set: speed, duration, force on the sample surface, and the amount of non-aqueous polishing medium such as propylene glycol or polishing oil sprayed on the surface. Then, the stated values should be adjusted and managed according to the catalog of the device and the material (type of aggregate, fibers, additions) to be polished. For the concrete sample to have a polished surface, this must be done in six steps [105], which can be summarized in Fig. 8.

After the above steps, the sample is ready for observation by microscopy. It should be noted that the steps taken to prepare the sample for examination by a light microscope to review the ITZ, such as the hardness test and some specific SEM photographs, are the same [49,102]. If all the sample preparation steps are done correctly and accurately in both methods of coating with conductive material and epoxy, all the ITZ areas can be correctly seen in the photos taken. In addition, no disturbance or noise in the photo was examined.

4. Results

4.1. Cutting and polishing

Fig. 9 shows the prepared and acceptable and unacceptable samples for the use and preparation of microscopic photographs. As it is apparent in Fig. 9-a, not using epoxy with the proper viscosity and not observing the correct ratio of mixing epoxy and hardener has caused the sample to become brittle and create cracks on its surface during the sample opening process. Other research has demonstrated that polyol-based epoxies have elasticity and impact strength and, as polyamine epoxy was utilized in this study, enhance the resistance of epoxy resin [106]. Also, the use of improper quality resin causes a change in the color of the sample. This color change causes errors in reading and analyzing the color spectrum in the photos taken from the sample. As observed, using epoxy with a viscosity of 550 cP (20 °C) produces the most outstanding results in terms of transparency and breaking resistance

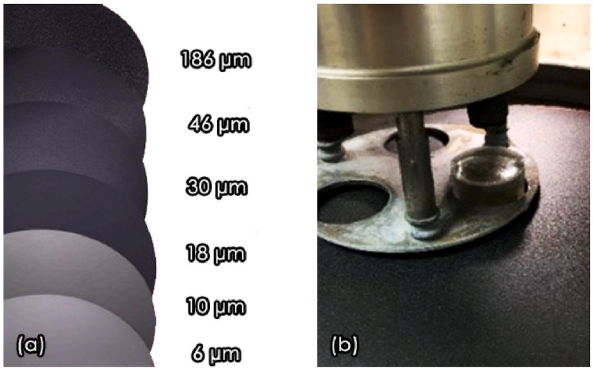

Fig. 8. Size of sandpaper and types of sandpaper (a), polishing machine (b).

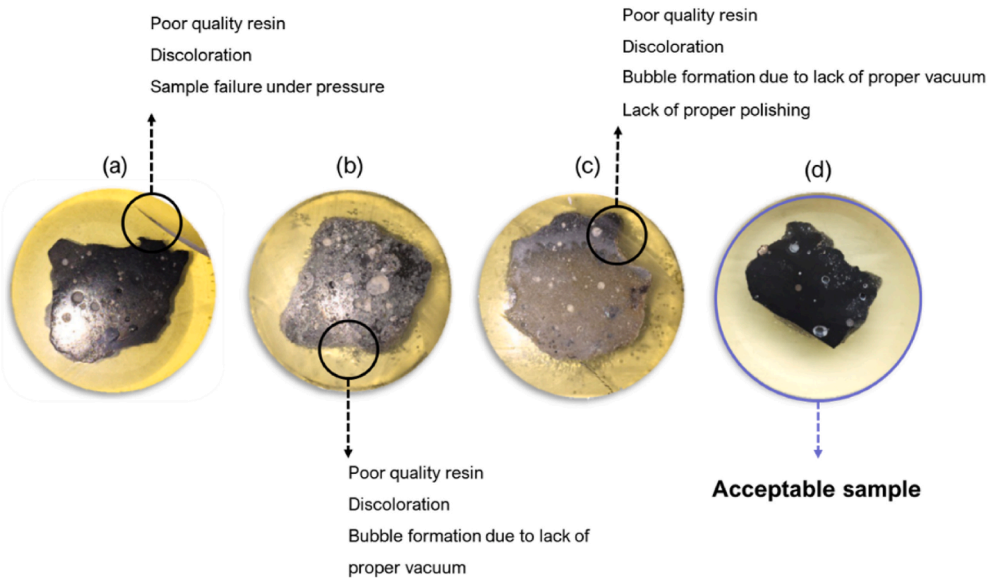

Fig. 9. Acceptable and unacceptable samples for use preparation of microscopic photographs.

among the epoxies tested [77]. Fig. 9-b shows a failure to pay attention to the steps of mixing temperature and following the use of a vacuum while covering the sample with epoxy has caused the formation of air bubbles around and on the sample's surface. According to some research, 50 °C is the ideal temperature for mixing epoxy, but temperatures between 50 °C and 75 °C have also been recommended [81,107]. This error is another disadvantage of the sample and will reduce the surface resistance of the sample during the polishing process. Failure to observe the six steps of sample polishing is another problem that can be seen in Fig. 9-c. This problem will have a very destructive effect on the photos taken of the sample and increase the error percentage in the image analysis due to the data loss in the photo. Fig. 9-d shows a complete and acceptable sample in terms of the type of resin, how to cover the sample with epoxy, and proper polishing.

Since sample polishing and how to do it is a critical issue in analyzing microscopic images, the effectiveness of this can be seen in Fig. 10. Fig. 10-a clearly shows the amount of data lost in the microscopic image taken due to the improper polishing of the sample surface. In this picture, the line of scratches left by the cutting blade after cutting the sample is also left. Also, the boundary line between the cement paste and other components in the photo cannot be seen due to improper polishing. Fig. 10-b is an acceptable photo for image processing because no noise or data loss is observed, and the border between cement paste and other components is also evident. Also, the number of existing scratches is minimal and can be ignored. As stated, the limitation of each method (SEM, TEM, and SPM) is in the depth of focus and accuracy of microscopic. Meanwhile, there is no limit to sample preparation, from the cutting and drying stage to selecting the sample surface coating method (EC, GC).

4.2. Analysis of electron microscope photos

As seen in the image taken by the electron microscope in Fig. 11-a, the sample's surface is not properly polished. The magnification of the photo (10 μm) and the smallness and delicacy of the existing scratches indicate that these scratches are related to improper polishing due to insufficient polishing time, the use of sandpaper with incorrect softness, or improper pressure on the surface of the sam-

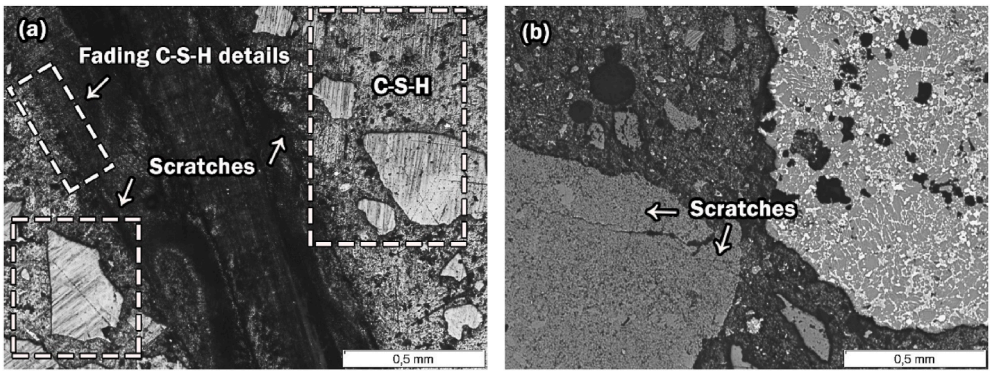

Fig. 10. Unpolished specimen and its effect on microscopic photographs.

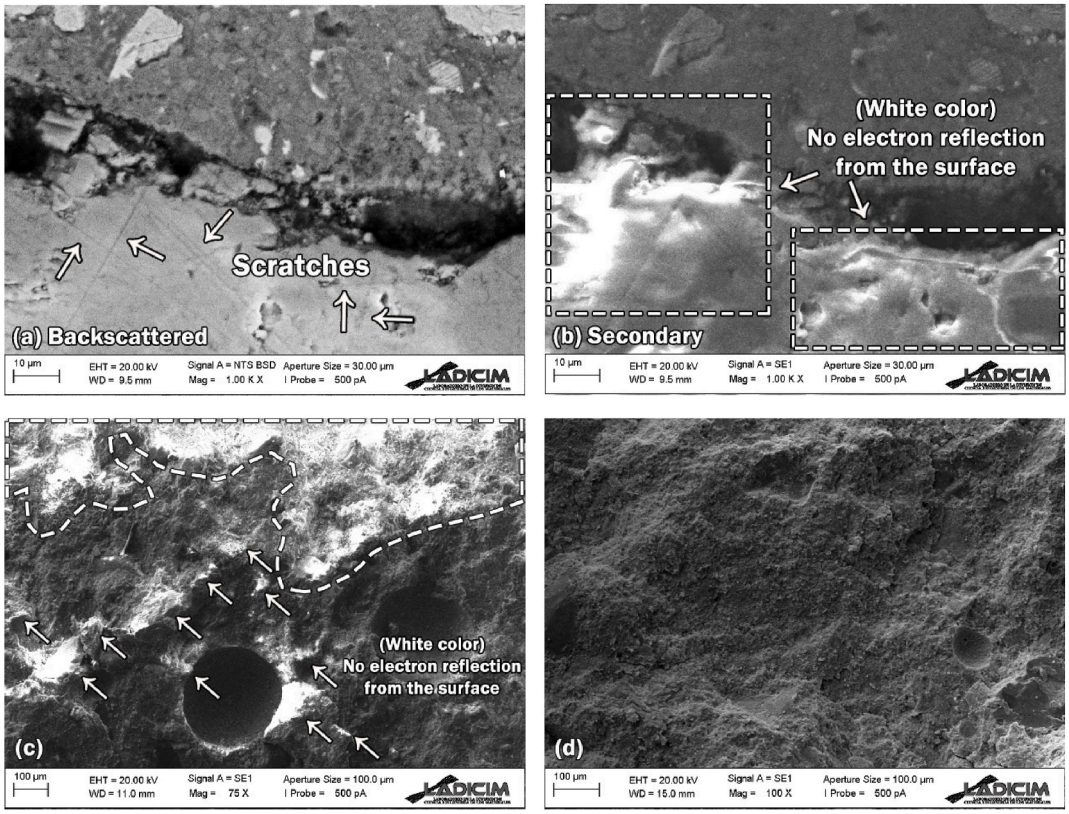

Fig. 11. Examples of factors affecting the photos taken by electron microscope: are the presence of scratches and improper polishing of sample (a), lack of reflection of electrons from the surface of the sample due to the presence of scratches and noise on the surface of sample (b), lack of reflection of electrons from the surface of the sample Due to improper and insufficient coverage of the sample surface with gold (c), adequate coverage of the sample surface with gold and the absence of any external noise (d).

ple. Therefore, they are left from the sixth stage, the final polishing stage. In addition to creating noise in the backscattered image of the sample, the scratches create noise in the secondary image of the sample shown in Fig. 11-b. This disorder is such that it does not allow electron reflection from the surface of the sample, and as a result, the photo cannot be examined in noisy areas. These areas that cannot reflect electrons usually turn white, making the data in these areas unusable. Failure to receive accurate information from the investigated surface can also be seen in coating the surface with gold or other suitable conductors. As Fig. 11-c shows, the lack of proper coating of the surface with gold or the use of improper quality gold has caused the surface of the sample not to have proper conductivity. As a result, electron reflection from the surface is not done correctly. The presence of white areas on the sample confirms this. Fig. 11-d shows a perfect secondary photo of the sample surface. In this photo, it can be seen that the steps of polishing and covering the surface of the sample by the conductor have been done well so that no noise or white dots that indicate the loss of photo data can be seen.

5. Conclusions

1. This study deals with the process of preparing concrete samples for the preparation of microscopic photos and the points and obstacles in this process. The following results have been obtained from the above discussion. Failure to use resin with appropriate viscosity and failure to observe the mixing ratio of resin and hardener causes low-quality, brittle and cloudy epoxy to be produced, which will hurt the process of the study.
2. Slow, long-term stirring of the two components of resin and hardener, as well as using a vacuum while covering the sample's surface with epoxy, significantly reduces the air bubbles in the sample covered with epoxy.
3. In order to have a sample surface free from noise and scratches, the six polishing steps must be completed according to the type of polishing machine and its recipe.
4. Improper coating by a strong conductor (gold in this study) causes no reflection of the electron from the surface of the sample, the creation of white areas, and the loss of data in that area from the photograph.
5. The remaining scratches due to improper polishing on the surface of the sample, in addition to creating noise in the backscattered photos, also cause white spots in the secondary photos, which affects the data obtained from the photo.

Credit author roles

Conceptualization: A. Aghajanian, A. Cimentada, M. Fayyaz, A.S. Brand, C. Thomas; Data curation: A. Aghajanian, A. Cimentada; M. Fayyaz Formal analysis: A. Aghajanian, A. Cimentada, , A.S. Brand, C. Thomas; Funding acquisition: A.S. Brand, C. Thomas; Project administration:, A.S. Brand, C. Thomas; Resources:, A.S. Brand, C. Thomas; Supervision:, A.S. Brand, C. Thomas; Validation: A. Aghajanian, A. Cimentada, , A.S. Brand, C. Thomas; Visualization: A. Aghajanian, A. Cimentada, , A.S. Brand, C. Thomas; Writing - original draft: A. Aghajanian, C. Thomas; Writing - review & editing A. Aghajanian, A. Cimentada, A.S. Brand, C. Thomas.

CRediT author statement

Author 1: Conceptualization; Methodology; Validation; Formal Analysis; Investigation; Data curation writing—original draft preparation; Data curation Writing – original draft; writing—review and editing; Supervision. **Author 2:** Conceptualization; Methodology; Formal analysis; Writing—initial draft preparation; Review and editing; Supervision; Project administration. **Author 3:** Methodology; Validation; Formal analysis; Writing—review, and editing; Supervision; Project administration. **Author 4:** Methodology; Validation; Formal analysis; Writing—review, and editing; Supervision; Project administration. All authors have read and agreed to the published version of the manuscript. All authors have read and agreed to the published version of the manuscript.

Declaration of competing interest

The authors declare that they have no known competing financial interests or personal relationships that could have appeared to influence the work reported in this paper.

Data availability

No data was used for the research described in the article.

Acknowledgments

The authors of this research would like to thank The LADICIM Laboratory of the Division of Science and Engineering of Materials for helping to take photos of equipment and use SEM laboratory devices.

References

[1] S. Diamond, J. Huang, The ITZ in concrete – a different view based on image analysis and SEM observations, Cem. Concr. Compos. 23 (2001) 179–188, https://doi.org/10.1016/S0958-9465(00)00065-2.
[2] Y. Gao, G. De Schutter, G. Ye, Z. Tan, K. Wu, The ITZ microstructure, thickness and porosity in blended cementitious composite: effects of curing age, water to binder ratio and aggregate content, Compos. B Eng. 60 (2014) 1–13, https://doi.org/10.1016/j.compositesb.2013.12.021.
[3] K.L. Scrivener, A.K. Crumbie, P. Laugesen, The interfacial transition zone (ITZ) between cement paste and aggregate in concrete, Interface Sci. 12 (2004 124 2004) 411–421, https://doi.org/10.1023/B:INTS.0000042339.92990.4C.
[4] J.C. Maso, Interfacial Transition Zone in Concrete, CRC Press, 1996, p. 200 https://doi.org/10.1201/9781482271560/INTERFACIAL-TRANSITION-ZONE-CONCRETE-MASO, 1st Editio.
[5] A. Palomo, P. Krivenko, I. Garcia-Lodeiro, E. Kavalerova, O. Maltseva, A. Fernández-Jiménez, A review on alkaline activation: new analytical perspectives, Mater. Construcción 64 (2014), https://doi.org/10.3989/mc.2014.00314.
[6] P. Tamayo, C. Thomas, J. Rico, A. Cimentada, J. Setién, J.A. Polanco, Review on neutron-absorbing fillers, Micro Nanostructured Compos Mater Neutron Shield Appl (2020) 25–52, https://doi.org/10.1016/b978-0-12-819459-1.00002-7.
[7] G.L. Golewski, Fracture performance of cementitious composites based on quaternary blended cements, Materials 15 (2022) 6023 https://doi.org/10.3390/MA15176023, 2022;15:6023.
[8] T. Akçaoğlu, M. Tokyay, T. Çelik, Assessing the ITZ microcracking via scanning electron microscope and its effect on the failure behavior of concrete, Cement Concr. Res. 35 (2005) 358–363, https://doi.org/10.1016/J.CEMCONRES.2004.05.042.
[9] C.S.S.R. Kumar, Transmission electron microscopy characterization of nanomaterials, Transm Electron Microsc Charact Nanomater (2014) 1–716, https://doi.org/10.1007/978-3-642-38934-4/COVER.
[10] Zhang P, Han S, Golewski GL, Wang X. Nanoparticle-reinforced building materials with applications in civil engineering. Https://DoiOrg/101177/1687814020965438 2014;12. https://doi.org/10.1177/1687814020965438.
[11] A. Aghajanian, C. Thomas, J. Sainz-Aja, The use of rice hush ash in eco-concrete, Struct Integr Recycl Aggreg Concr Prod with Fill Pozzolans (2022) 171 https://doi.org/10.1016/B978-0-12-824105-9.00006-8, –97.
[12] D.M. Gil, G.L. Golewski, Potential of siliceous fly ash and silica fume as a substitute for binder in cementitious concretes, E3S Web Conf 49 (2018) 00030, https://doi.org/10.1051/E3SCONF/20184900030.
[13] M.P. Lutz, P.J.M. Monteiro, R.W. Zimmerman, Inhomogeneous interfacial transition zone model for the bulk modulus of mortar, Cement Concr. Res. 27 (1997) 1113–1122, https://doi.org/10.1016/S0008-8846(97)00086-0.
[14] A. Aghajanian, C. Thomas, K. Behfarnia, Effect of micro-silica addition into electric arc furnace steel slag eco-efficient concrete, Appl. Sci. 11 (2021) 4893 https://doi.org/10.3390/APP11114893, 2021;11:4893.
[15] Z. Pi, H. Xiao, R. Liu, M. Liu, Quantitative analysis of steel fiber-matrix ITZ and multi-scale enhancement mechanism of SFRC, Mater Struct Constr 54 (2021) 1–18, https://doi.org/10.1617/S11527-021-01825-4/FIGURES/14.
[16] X.H. Wang, S. Jacobsen, S.F. Lee, J.Y. He, Z.L. Zhang, Effect of silica fume, steel fiber and ITZ on the strength and fracture behavior of mortar, Mater Struct Constr 43 (2010) 125–139, https://doi.org/10.1617/S11527-009-9475-1/FIGURES/9.
[17] G.L. Golewski, S. Walker, N.D. Browning, Green concrete based on quaternary binders with significant reduced of CO2 emissions, Energies 14 (2021) 4558 https://doi.org/10.3390/EN14154558, 2021;14:4558.
[18] S.W. Ziegeldorf, H.K. Hilsdorf, A review of the cement-aggregate bond, Cement Concr. Res. 10 (1980) 5.
[19] S. He, Z. Li, E.H. Yang, Quantitative characterization of anisotropic properties of the interfacial transition zone (ITZ) between microfiber and cement paste, Cement Concr. Res. 122 (2019) 136–146, https://doi.org/10.1016/J.CEMCONRES.2019.05.007.
[20] A.S. Brand, E.O. Fanijo, A review of the influence of steel furnace slag type on the properties of cementitious composites, Appl. Sci. 10 (2020) 1–27, https://doi.org/10.3390/app10228210.
[21] A. Aghajanian, C. Thomas, J. Sainz-Aja, A. Cimentada, Colemanite filler from wastes in recycled concrete, Struct Integr Recycl Aggreg Concr Prod with Fill Pozzolans (2022) 79–103, https://doi.org/10.1016/B978-0-12-824105-9.00007-X.

[22] J.J. Kim, D.J. Kim, S.T. Kang, J.H. Lee, Influence of sand to coarse aggregate ratio on the interfacial bond strength of steel fibers in concrete for nuclear power plant, Nucl. Eng. Des. 252 (2012) 1–10, https://doi.org/10.1016/j.nucengdes.2012.07.004.
[23] J.C. Maso, Interfaces in cementitious composites, Interfaces Cem Compos (1992), https://doi.org/10.1201/9781482271256.
[24] P.R. Rangaraju, J. Olek, S. Diamond, An investigation into the influence of inter-aggregate spacing and the extent of the ITZ on properties of Portland cement concretes, Cement Concr. Res. 40 (2010) 1601–1608, https://doi.org/10.1016/J.CEMCONRES.2010.07.002.
[25] A. Hussin, C. Poole, Petrography evidence of the interfacial transition zone (ITZ) in the normal strength concrete containing granitic and limestone aggregates, Construct. Build. Mater. 25 (2011) 2298–2303, https://doi.org/10.1016/J.CONBUILDMAT.2010.11.023.
[26] Y. Ke, S. Ortola, A.L. Beaucour, H. Dumontet, Identification of microstructural characteristics in lightweight aggregate concretes by micromechanical modelling including the interfacial transition zone (ITZ), Cement Concr. Res. 40 (2010) 1590–1600, https://doi.org/10.1016/J.CEMCONRES.2010.07.001.
[27] P. Tamayo, A. Aghajanian, J. Rico, J. Setién, J.A. Polanco, C. Thomas, Characterization of the adherence strength and the aggregate-paste bond of prestressed concrete with siderurgical aggregates, J. Build. Eng. 54 (2022) 104595, https://doi.org/10.1016/J.JOBE.2022.104595.
[28] A. Aghajanian, A. Cimentada, K. Behfarnia, A.S. Brand, C. Thomas, Microstructural analysis of siderurgical aggregate concrete reinforced with fibers, J. Build. Eng. (2022) 105543, https://doi.org/10.1016/J.JOBE.2022.105543.
[29] A. Leemann, R. Loser, B. Münch, Influence of cement type on ITZ porosity and chloride resistance of self-compacting concrete, Cem. Concr. Compos. 32 (2010) 116–120, https://doi.org/10.1016/J.CEMCONCOMP.2009.11.007.
[30] J jun Zheng, H.S. Wong, N.R. Buenfeld, Assessing the influence of ITZ on the steady-state chloride diffusivity of concrete using a numerical model, Cement Concr. Res. 39 (2009) 805–813, https://doi.org/10.1016/J.CEMCONRES.2009.06.002.
[31] J. Zheng, X. Zhou, X. Jin, An n-layered spherical inclusion model for predicting the elastic moduli of concrete with inhomogeneous ITZ, Cem. Concr. Compos. 34 (2012) 716–723, https://doi.org/10.1016/J.CEMCONCOMP.2012.01.011.
[32] G.L. Golewski, An extensive investigations on fracture parameters of concretes based on quaternary binders (QBC) by means of the DIC technique, Construct. Build. Mater. 351 (2022) 128823, https://doi.org/10.1016/J.CONBUILDMAT.2022.128823.
[33] J.M. Manso, J.A. Polanco, M. Losañez, J.J. González, Durability of concrete made with EAF slag as aggregate, Cem. Concr. Compos. 28 (2006) 528–534, https://doi.org/10.1016/j.cemconcomp.2006.02.008.
[34] A.S. Brand, J.R. Roesler, Steel furnace slag aggregate expansion and hardened concrete properties, Cem. Concr. Compos. 60 (2015) 1–9, https://doi.org/10.1016/j.cemconcomp.2015.04.006.
[35] G.L. Golewski, Comparative measurements of fracture toughgness combined with visual analysis of cracks propagation using the DIC technique of concretes based on cement matrix with a highly diversified composition, Theor. Appl. Fract. Mech. 121 (2022) 103553, https://doi.org/10.1016/J.TAFMEC.2022.103553.
[36] J.A. Sainz-Aja, M. Sanchez, L. Gonzalez, P. Tamayo, G.G. Del Angel, A. Aghajanian, et al., Recycled polyethylene fibres for structural concrete, Appl. Sci. 12 (2022) 2867 https://doi.org/10.3390/APP12062867, 2022;12:2867.
[37] I.Z. Yildirim, M. Prezzi, Chemical, mineralogical, and morphological properties of steel slag, Adv. Civ. Eng. 2011 (2011), https://doi.org/10.1155/2011/463638.
[38] G.L. Golewski, B. Szostak, Strength and microstructure of composites with cement matrixes modified by fly ash and active seeds of C-S-H phase, Struct. Eng. Mech. 82 (2022) 543–556, https://doi.org/10.12989/SEM.2022.82.4.543.
[39] G.G. Del Angel, A. Aghajanian, P. Tamayo, J. Rico, C. Thomas, Siderurgical aggregate cement-treated bases and concrete using foundry sand, Appl. Sci. 11 (2021) 435 https://doi.org/10.3390/APP11010435, 2021;11:435.
[40] A.S. Brand, E.O. Fanijo, A review of the influence of steel furnace slag type on the properties of cementitious composites, Appl. Sci. 10 (2020) 8210 https://doi.org/10.3390/APP10228210, 2020;10:8210.
[41] W. Langer, USGS open-file report 2011-1119: aggregate resource availability in the conterminous United States, including suggestions for addressing shortages, quality, and environmental concerns, US Geol Surv Open-File Rep (2011) 1119 2011:87 Vol. I. https://pubs.usgs.gov/of/2011/1119/. (Accessed 26 October 2022). accessed.
[42] L. Gallagher, P. Peduzzi, Sand and Sustainability: Finding New Solutions for Environmental Governance of Global Sand Resources, 2019.
[43] W. Criteria, R. Aggregates, UEPG guidance end of waste criteria for recycled aggregates from, Construction & Demolition Waste (2022) 1–24.
[44] Business E, Manual S. Production of European Aggregates n.d.;27:1–6.
[45] A.S. Brand, J.R. Roesler, Interfacial transition zone of cement composites with steel furnace slag aggregates, Cem. Concr. Compos. 86 (2018) 117–129, https://doi.org/10.1016/J.CEMCONCOMP.2017.11.012.
[46] S. Bradbury, P. Evennett, Contrast techniques in light microscopy, Contrast Tech Light Microsc (2020), https://doi.org/10.1201/9781003076834.
[47] R.F. Egerton, Physical principles of electron microscopy: an introduction to TEM, SEM, and AEM, in: Phys Princ Electron Microsc an Introd to TEM, second ed., SEM, AEM, 2016, pp. 1–196 https://doi.org/10.1007/978-3-319-39877-8/COVER, Second Ed.
[48] Kohl Reimer, 9780387347585_Toc, 5, Springer Ser Opt Sci, 2008.
[49] A.S. H. Optical microscopy. Concise Encycl Mater Charact n.d.:286–92. https://www.scopus.com/record/display.uri?eid=2-s2.0-85080803821&origin=inward&featureToggles=FEATURE_NEW_DOC_DETAILS_EXPORT:1 (accessed March 16, 2022).
[50] D.H. Campbell, Microscopical Examination and Interpretation of Portland Cement and Clinker: Portland Cement Association, 1999.
[51] K.L. Scrivener, P.L. Pratt, Backscattered electron images of polished cement sections in the scanning electron microscope, Proc Int Conf Cem Microsc (1984) 145–155 (accessed March 16, 2022). https://infoscience.epfl.ch/record/166495.
[52] D. Stokes, Royal Microscopical Society (Great Britain), Principles and Practice of Variable Pressure/environmental Scanning Electron Microscopy, VP-ESEM), 2008, p. 221.
[53] K. Vos, N. Vandenberghe, J. Elsen, Surface textural analysis of quartz grains by scanning electron microscopy (SEM): from sample preparation to environmental interpretation, Earth Sci. Rev. 128 (2014) 93–104, https://doi.org/10.1016/J.EARSCIREV.2013.10.013.
[54] F. Orsini, A. Du Pasquier, B. Beaudoin, J.M. Tarascon, M. Trentin, N. Langenhuizen, et al., In situ Scanning Electron Microscopy (SEM) observation of interfaces within plastic lithium batteries, J. Power Sources 76 (1998) 19–29, https://doi.org/10.1016/S0378-7753(98)00128-1.
[55] L. Reimer, Scanning electron microscopy: physics of image formation and microanalysis, in: Meas Sci Technol, Second Edition, 2000, p. 1826 https://doi.org/10.1088/0957-0233/11/12/703, 11.
[56] S El Abed, S.K. Ibnsouda, H. Latrache, F. Hamadi, Scanning electron microscopy (SEM) and environmental SEM: suitable tools for study of adhesion stage and biofilm formation, Scanning Electron. Microsc. (2012), https://doi.org/10.5772/34990.
[57] B. Fultz, J.M. Howe, Transmission electron microscopy and diffractometry of materials, Transm Electron Microsc Diffractometry Mater 1–758 (2008), https://doi.org/10.1007/978-3-540-73886-2/COVER.
[58] Y.U. Heo, Comparative study on the specimen thickness measurement using EELS and CBED methods, Appl Microsc 50 (2020), https://doi.org/10.1186/s42649-020-00029-4.
[59] S. Li, Y. Chang, Y. Wang, Q. Xu, B. Ge, A review of sample thickness effects on high-resolution transmission electron microscopy imaging, Micron 130 (2020) 102813, https://doi.org/10.1016/J.MICRON.2019.102813.
[60] S. Sadamatsu, M. Tanaka, K. Higashida, S. Matsumura, Transmission electron microscopy of bulk specimens over 10 μm in thickness, Ultramicroscopy 162 (2016) 10–16, https://doi.org/10.1016/J.ULTRAMIC.2015.09.001.
[61] Thickness requirements of TEM samples for EELS/EFTEM/EDS/HAADF STEM, n.d. https://www.globalsino.com/EM/page4487.html (Accessed 27 October 2022) accessed.
[62] L. Reimer, Transmission Electron Microscopy 36 (1984), https://doi.org/10.1007/978-3-662-13553-2.
[63] J. Gomez-Herrero, R. Reifenberger, Scanning probe microscopy, Encycl Condens Matter Phys 172–82 (2005), https://doi.org/10.1016/B0-12-369401-9/00585-4.
[64] B.L. Ramakrishna, E.W. Ong, Surface evaluation by atomic force microscopy, Encycl Mater Sci Technol (2001) 9030 https://doi.org/10.1016/B0-08-043152-6/01628-4, –6.

[65] M. Afrand, R. Ranjbarzadeh, Hybrid nanofluids preparation method, Hybrid Nanofluids Convect Heat Transf 49–99 (2020), https://doi.org/10.1016/B978-0-12-819280-1.00002-1.

[66] C.J. Roberts, M.C. Davies, S.J.B. Tendler, P.M. Williams, Scanning probe microscopy, applications, Encycl Spectrosc Spectrom (1999) 2051 https://doi.org/10.1006/RWSP.2000.0271, 9.

[67] Dale E. Newbury, Scanning electron microscopy and X-ray microanalysis - joseph I. Goldstein n.d Joseph R. Michael, Nicholas W.M. Ritchie, John Henry J. Scott, David C. Joy - Google Books (2023) Vol. I, Scanning + electron + microscopy + and + X-ray + microanalysis. + Springer, + 2017.&ots = 36RG9lIlso&sig = sOuYImTcc_lmvYODAFf4J0HCeGw#v = onepage&q&f = false (accessed January 4, 2023) https://books.google.com/books?hl = en&lr = &id = D0I_DwAAQBAJ&oi = fnd&pg = PR5&dq = Goldstein, + Joseph + I.

[68] A.K. Singh, Experimental methodologies for the characterization of nanoparticles, Eng Nanoparticles 125–70 (2016), https://doi.org/10.1016/B978-0-12-801406-6.00004-2.

[69] B.J. Inkson, Scanning electron microscopy (SEM) and transmission electron microscopy (TEM) for materials characterization, Mater Charact Using Nondestruct Eval Methods (2016) 17–43, https://doi.org/10.1016/B978-0-08-100040-3.00002-X.

[70] A.M. Kashi, K. Tahermanesh, S. Chaichian, M.T. Joghataei, S.M. Tavangar, A. Sadat, et al., How to prepare biological samples and live tissues for scanning electron microscopy (SEM), Galen Med J 3 (2014) 63–80.

[71] Difference for scanning electron microscopy | SEM vs TEM, Mahamax (2019) Web page. https://mahamax.com/تفاوت-بین-روش-میکروسکوپ-الکترونی-روبشی-و-عبوری/. (Accessed 16 March 2022). accessed.

[72] C.E. Lyman, J.I. Goldstein, A.D. Romig, P. Echlin, D.C. Joy, D.E. Newbury, et al., Scanning electron microscopy, X-ray microanalysis, and analytical electron microscopy, Scanning Electron Microsc X-Ray Microanal Anal Electron Microsc (1990), https://doi.org/10.1007/978-1-4613-0635-1.

[73] May C. Epoxy Resins : Chemistry and Technology, Second Edition (n.d).

[74] P. Echlin, Handbook of sample preparation for scanning electron microscopy and X-ray microanalysis, Handb Sample Prep Scanning Electron Microsc X-Ray Microanal (2009), https://doi.org/10.1007/978-0-387-85731-2.

[75] Reactive Diluent for Epoxy Resin, 1992.

[76] A. Sinha, N. Islam Khan, S. Das, J. Zhang, S. Halder, Effect of reactive and non-reactive diluents on thermal and mechanical properties of epoxy resin, High Perform. Polym. 30 (2018) 1159–1168 https://doi.org/10.1177/0954008317743307/ASSET/IMAGES/LARGE/10.1177_0954008317743307-FIG2 (JPEG).

[77] I. Miturska, A. Rudawska, M. Müller, M. Hromasová, The influence of mixing methods of epoxy composition ingredients on selected mechanical properties of modified epoxy construction materials, Materials 14 (2021) 411 https://doi.org/10.3390/MA14020411, 2021;14:411.

[78] J.A. Brydson, Epoxide resins, Plast Mater 744–77 (1999), https://doi.org/10.1016/B978-075064132-6/50067-X.

[79] A.R. Jagtap, A. More, Developments in reactive diluents: a review, Polym. Bull. 79 (2021 798 2021) 5667–5708, https://doi.org/10.1007/S00289-021-03808-5.

[80] M. Khalina, M.H. Beheshty, A. Salimi, The effect of reactive diluent on mechanical properties and microstructure of epoxy resins, Polym. Bull. 76 (2019) 3905–3927, https://doi.org/10.1007/S00289-018-2577-6/FIGURES/11.

[81] G. Gibson, Epoxy resins, Brydson's Plast Mater Eighth Ed (2017) 773–797, https://doi.org/10.1016/B978-0-323-35824-8.00027-X.

[82] P. Castan, T. Freres, Process for the Manufacture of Thermosetting Synthetic Resins by the Polymerization of Alkylene Oxide Derivatives, 1944, p. 790.

[83] S.J. Monte, Diluents and Viscosity Modifiers for Epoxy Resins, 211–6, 1998, https://doi.org/10.1007/978-94-011-5862-6_24.

[84] S.R. Sandler, W. Karo, Epoxy resins, Polym Synth (1994) 87–128, https://doi.org/10.1016/B978-0-08-092555-4.50007-4.

[85] H. Schneider, N. Siegenthaler, Epoxy Resin Mixtures Containing Advancement Catalysts, 1994, p. 521.

[86] M. Narmluk, T. Nawa, Effect of fly ash on the kinetics of Portland cement hydration at different curing temperatures, Cement Concr. Res. 41 (2011) 579–589, https://doi.org/10.1016/J.CEMCONRES.2011.02.005.

[87] N.C. Collier, J.H. Sharp, N.B. Milestone, J. Hill, I.H. Godfrey, The influence of water removal techniques on the composition and microstructure of hardened cement pastes, Cement Concr. Res. 38 (2008) 737–744, https://doi.org/10.1016/J.CEMCONRES.2008.02.012.

[88] J.J. Thomas, J.J. Biernacki, J.W. Bullard, S. Bishnoi, J.S. Dolado, G.W. Scherer, et al., Modeling and simulation of cement hydration kinetics and microstructure development, Cement Concr. Res. 41 (2011) 1257–1278, https://doi.org/10.1016/J.CEMCONRES.2010.10.004.

[89] H.M. Jennings, J.W. Bullard, J.J. Thomas, J.E. Andrade, J.J. Chen, G.W. Scherer, Characterization and modeling of pores and surfaces in cement paste : correlations to processing and properties, J. Adv. Concr. Technol. 6 (2008) 5–29, https://doi.org/10.3151/JACT.6.5.

[90] K.K. Aligizaki, Pore structure of cement-based materials : testing, interpretation and requirements, Pore Struct Cem Mater (2005), https://doi.org/10.1201/9781482271959.

[91] C. Gallé, Effect of drying on cement-based materials pore structure as identified by mercury intrusion porosimetry: a comparative study between oven-, vacuum-, and freeze-drying, Cement Concr. Res. 31 (2001) 1467–1477, https://doi.org/10.1016/S0008-8846(01)00594-4.

[92] A. Korpa, R. Trettin, The influence of different drying methods on cement paste microstructures as reflected by gas adsorption: comparison between freeze-drying (F-drying), D-drying, P-drying and oven-drying methods, Cement Concr. Res. 36 (2006) 634–649, https://doi.org/10.1016/J.CEMCONRES.2005.11.021.

[93] J. Zhang, G.W. Scherer, Comparison of methods for arresting hydration of cement, Cement Concr. Res. 41 (2011) 1024–1036, https://doi.org/10.1016/J.CEMCONRES.2011.06.003.

[94] I ap Gwynn, Handbook of sample preparation for scanning electron microscopy and X-ray microanalysis, Patrick Echlin. Springer, New York. Microsc. Microanal. (2009) 330 https://doi.org/10.1017/S1431927609991152, 978-0-387-85730-5(Hardcover), 2010;16:358–359.

[95] D.E. Newbury, D.C. Joy, P. Echlin, C.E. Fiori, J.I. Goldstein, Advanced scanning electron microscopy and X-ray microanalysis, Adv Scanning Electron Microsc X-Ray Microanal (1986), https://doi.org/10.1007/978-1-4757-9027-6.

[96] J. Gruenberg, D.R. Allred, I.W. Sherman, Scanning electron microscope-analysis of the protrusions (knobs) present on the surface of Plasmodium falciparum-infected erythrocytes, J. Cell Biol. 97 (1983) 795–802, https://doi.org/10.1083/JCB.97.3.795.

[97] H. Seiler, Secondary electron emission in the scanning electron microscope, J. Appl. Phys. 54 (1998) R1, https://doi.org/10.1063/1.332840.

[98] M.R. Scheinfein, J. Unguris, M.H. Kelley, D.T. Pierce, R.J. Celotta, Scanning electron microscopy with polarization analysis (SEMPA), Rev. Sci. Instrum. 61 (1998) 2501, https://doi.org/10.1063/1.1141908.

[99] K.C.A. Smith, C.W. Oatley, Scanning Electron Microscopy in Concrete Petrography, 2000.

[100] R.V. Balendran, H.W. Pang, H.X. Wen, Use of scanning electron microscopy in concrete studies, Struct. Surv. 16 (1998) 146–153, https://doi.org/10.1108/02630809810232718/FULL/XML.

[101] K.C.A. Smith, C.W. Oatley, The scanning electron microscope and its fields of application, Br. J. Appl. Phys. 6 (1955) 391, https://doi.org/10.1088/0508-3443/6/11/304.

[102] D. Jana, Sample preparation techniques in petrographic examinations of construction materials: a state-of-the-art review, Int Cem Microsc Assoc - 28th Int Conf Cem Microsc (2006 2006) 22–69.

[103] L. Evangelista, M. Guedes, Microstructural studies on recycled aggregate concrete, New Trends Eco-Efficient Recycl Concr (2019) 425–451, https://doi.org/10.1016/B978-0-08-102480-5.00014-2.

[104] Rachel J. Detwiler; Laura J. Powers; Ulla Hjorth Jakobsen; Wase U. Ahmed; Karen L. Scrivener; and Knut O. KjellsenPreparing specimens for microscopy, Concr Int n.d. 23 51–58.

[105] A. Aghajanian, A. Cimentada, C. Thomas, Siderurgical aggregates concrete ITZ: sample preparation, 6th Brazilian Conf Compos Mater (2022) 382 https://doi.org/10.29327/566492, –6.

[106] M. Khalina, M.H. Beheshty, A. Salimi, The effect of reactive diluent on mechanical properties and microstructure of epoxy resins, Polym. Bull. 76 (2019) 3905–3927, https://doi.org/10.1007/S00289-018-2577-6/METRICS.

[107] A. Rudawska, I. Haniecka, M. Jaszek, D. Stefaniuk, The influence of adhesive compounds biochemical modification on the mechanical properties of adhesive joints, Polymers 10 (2018) 344 https://doi.org/10.3390/POLYM10040344, 2018;10:344.